PAPER

A new iron-based metal–organic framework with enhancing catalysis activity for benzene hydroxylation†

Thach N. Tu, [ID] *[ab] Hue T. T. Nguyen,[bc] Huong T. D. Nguyen, [ID][c] My V. Nguyen, [ID][c] Trinh D. Nguyen, [ID][a] Nhung Thi Tran[d] and Kwon Taek Lim [ID][e]

A new Fe-based metal–organic framework (MOF), termed Fe-TBAPy Fe$_2$(OH)$_2$(TBAPy)·4.4H$_2$O, was solvothermally synthesized. Structural analysis revealed that Fe-TBAPy is built from [Fe(OH)(CO$_2$)$_2$]$_\infty$ rod-shaped SBUs (SBUs = secondary building units) and 1,3,6,8-tetrakis(p-benzoate)pyrene (TBAPy^{4-}) linker to form the **frz** topological structure highlighted by 7 Å channels and 3.4 Å narrow pores sandwiching between the pyrene cores of TBAPy^{4-}. Consequently, Fe-TBAPy was used as a recyclable heterogeneous catalyst for benzene hydroxylation. Remarkably, the catalysis reaction resulted in high phenol yield and selectivity of 64.5% and 92.9%, respectively, which are higher than that of the other Fe-based MOFs and comparable with those of the best-performing heterogeneous catalysts for benzene hydroxylation. This finding demonstrated the potential for the design of MOFs with enhancing catalysis activity for benzene hydroxylation.

1. Introduction

Phenol is an important chemical for the production of bakelite and phenolic resins. Currently, the global production of phenol is over 7.2 megatons per year.[1,2] Traditionally, phenol is produced from benzene by three-step cumene process, which suffers low yield (∼5%),[3] high energy consumption,[4] and generates the explosive cumene hydroperoxide intermediate,[1] as well as the unnecessary by-products (*e.g.* acetone, α-methyl-styrene).[5] Recently, significant efforts have been devoted to developing the greener and safer one-step hydroxylation protocol for production of phenol from benzene.[6] In this regard, various catalysts have been used; however, the phenol yields are low for most catalytic systems, for examples FeOCl (43.5%);[1] VPO@GO (32.8%);[7] Fe–ZSM-5 (22.9%);[8] Cu$_2$O-8/dG (19.2%)[9] (see ESI, Table S3†). On the contrary, only a few examples showed the quantitative yield of phenol.[10,11] Indeed, this could be attributed to the fact that phenol is more reactive toward oxidation than benzene.[6]

Metal–organic frameworks (MOFs) are a new class of porous extended materials assembled from well-defined inorganic and organic building units, which link together by strong bonds to shape the periodic structure. Attributing to the flexibility in choosing the building blocks, various MOFs with adjustable pore sizes and shapes as well as tunable internal chemical environments are designed and synthesized.[12] Up to now, a vast number of MOFs are synthesized and used in a wide range of applications including but not limited to gas and vapour storage/separation,[13–15] proton conduction,[16–18] catalysis,[19,20] sensing,[21–23] and drug delivery.[24,25] Recently, various Fe-based MOFs were synthesized and exhibited interesting properties.[26–29] Especially, the employment of Fe-based MOFs as the catalysts for the direct C–H bond activation showed excellent performance.[30–33] On the other hand, studies using MOFs for benzene hydroxylation are rarely reported. Indeed, an example employing MIL-100(Fe) and MIL-68(Fe) for benzene hydroxylation showed less than 30.6% benzene conversion.[34,35]

With this in mind, we wish to report the synthesis and characterization of a new iron-based MOF, termed Fe-TBAPy. Structural analysis of Fe-TBAPy, formulated as Fe$_2$(OH)$_2$(TBAPy)·4.4H$_2$O, revealed that Fe-TBAPy is built from [Fe(OH)(CO$_2$)$_2$]$_\infty$ rod-shaped SBUs linked by TBAPy^{4-} to form the **frz** topological framework.[36] This structure is highlighted by 7 Å channels along the O$_z$ axis and 3.4 Å pores sandwiching between the pyrene cores of TBAPy^{4-}. With this feature, Fe-TBAPy was employed for benzene hydroxylation reaction. As

^{a}Nguyen Tat Thanh University, 300A Nguyen Tat Thanh Street, District 4, Ho Chi Minh City 755414, Vietnam. E-mail: tnthach@ntt.edu.vn

^{b}Center for Innovative Materials and Architectures (INOMAR), Vietnam National University-Ho Chi Minh (VNU-HCM), Ho Chi Minh City 721337, Vietnam. E-mail: tnthach@inomar.edu.vn

^{c}University of Science, Vietnam National University-Ho Chi Minh (VNU-HCM), Ho Chi Minh City 721337, Vietnam

^{d}Ho Chi Minh City University of Technology and Education, 01 Vo Van Ngan Street, Linh Chieu Ward, Thu Duc District, Ho Chi Minh City 720100, Vietnam

^{e}Department of Display Engineering, Pukyong National University, Busan, 608-737, South Korea

† Electronic supplementary information (ESI) available: Full synthesis and characterization, crystallographic data, catalysis study of Fe-TBAPy. See DOI: 10.1039/c9ra03287h

a result, the catalysis reaction using 1.0 mol% Fe-TBAPy proceeded with the optimized phenol yield and selectivity of 64.5% and 92.9%, respectively. This value is higher than that of the other iron-based MOFs (*e.g.* MIL-100(Fe), MIL-126, MIL-68(Fe), MIL-88(Fe), and VNU-20)[37–41] and comparable with those of the best-performing heterogeneous catalysts for benzene hydroxylation.

2. Experimental

Chemicals

N,*N*-Dimethylformamide (DMF), acetic acid (CH_3COOH, 98%), dichloromethane (CH_2Cl_2, 99.9%), and anhydrous methanol (MeOH, 99.8%), were obtained from EMD Millipore Chemicals. Iron chloride anhydrous ($FeCl_2$, 98%) were obtained from Acros Organic. Palladium-tetrakis(triphenylphosphine) (99%), benzene (99.9%), toluene (99.8%) H_2O_2 (30 wt%) were purchased from Sigma-Aldrich. 1,3,6,8-tetrabromopyrene (purity > 98%) and methyl 4-boronobenzoate (purity > 96%) were purchased from Tokyo Chemical Industry Co. All starting materials and solvents were used without further purification. Fe-based MOFs and H_4TBAPy were synthesized according to the published procedures.[37–42]

Synthesis of Fe-TBAPy

A mixture of anhydrous $FeCl_2$ (0.050 g, 0.39 mmol) and H_4TBAPy (0.040 g, 0.058 mmol) was dissolved in 15 mL DMF. Subsequently, acetic acid (250 μL) was added and the solution was sonicated for 5 minutes, divided into glass tubes (1.5 mL each tube), which were flame-sealed under ambient atmosphere and temperature. Following this, the tubes were placed in an isothermal oven at 180 °C for one day. The resulting yellow micro-crystalline product was collected, washed with DMF (10 mL), methanol (10 mL) and dichloromethane (10 mL) for 3 d, respectively. During the solvent-exchange, each solvents were

decanted and replenished 5 times per day. Finally, the product was evacuated under vacuum (10^{-3} torr) at room temperature to yield Fe-TBAPy (67% yield, based on H_4TBAPy). Elemental analysis (EA) of activated sample: calcd for $Fe_2C_{44}H_{32.8}O_{14.4} = Fe_2(OH)_2(TBAPy)\cdot4.4H_2O$: C, 58.46; H, 3.41; N, 0%. Found: C, 58.5; H, 3.69; N, 0.31%. FT-IR (ATR): 1605 (m); 1580 (m); 1516 (m); 1380 (s); 1179 (m); 1144 (w); 1103 (w); 1019 (w); 1007 (m); 979 (w); 900 (w); 862 (m); 742 (m); 816 (m); 784 (m); 767 (m); and 716 (m); 641 (m) (Fig. S5†).

3. Results and discussion

Synthesis and characterization of Fe-TBAPy

A mixture of H_4TBAPy and $FeCl_2$ was dissolved in DMF in the presence of CH_3COOH and isothermally heated at 180 °C for 24 h to yield yellow micro-crystalline material of Fe-TBAPy. The as-synthesized material was further collected, washed and activated under dynamic vacuum at room temperature. The PXRD pattern of the activated sample was collected and indexed (Fig. S2†). The resulted unit cell parameters were refined against the experimental profile by Pawley method. Accordingly, Fe-TBAPy is found to crystallize in the monoclinic space group, $P2/c$ (no. 13), with unit cell parameters, $a = 14.2972$; $b = 15.5453$; $c = 14.0069$ Å and $\beta = 84.79°$ (Section S4†). We found that the obtained unit cell parameters are similar to that of the distorted structures of $[In_2(OH)_2(TBAPy)]$.[42] Therefore, a modelled structure of Fe-TBAPy was built based on the atomic connectivity of $[In_2(OH)_2(TBAPy)]$ (Table S1†). With this structural model, the full range Rietveld refinement against the experimental profile was performed to optimize the atom positions in the unit cell. Finally, the structure was successfully refined with low R-values ($2\theta = 2–80°$, $R_p = 7.53\%$ and $R_{wp} = 9.92\%$, Fig. 2 and S3†). The refined structure clearly showed that Fe-TBAPy is built from the commonly observed $[Fe(OH)(CO_2)_2]_\infty$ rod-shaped SBUs (Fig. 1a),[39,43,44] which are connected by $TBAPy^{4-}$ linkers (Fig. 1b) to expand into the **frz** topological
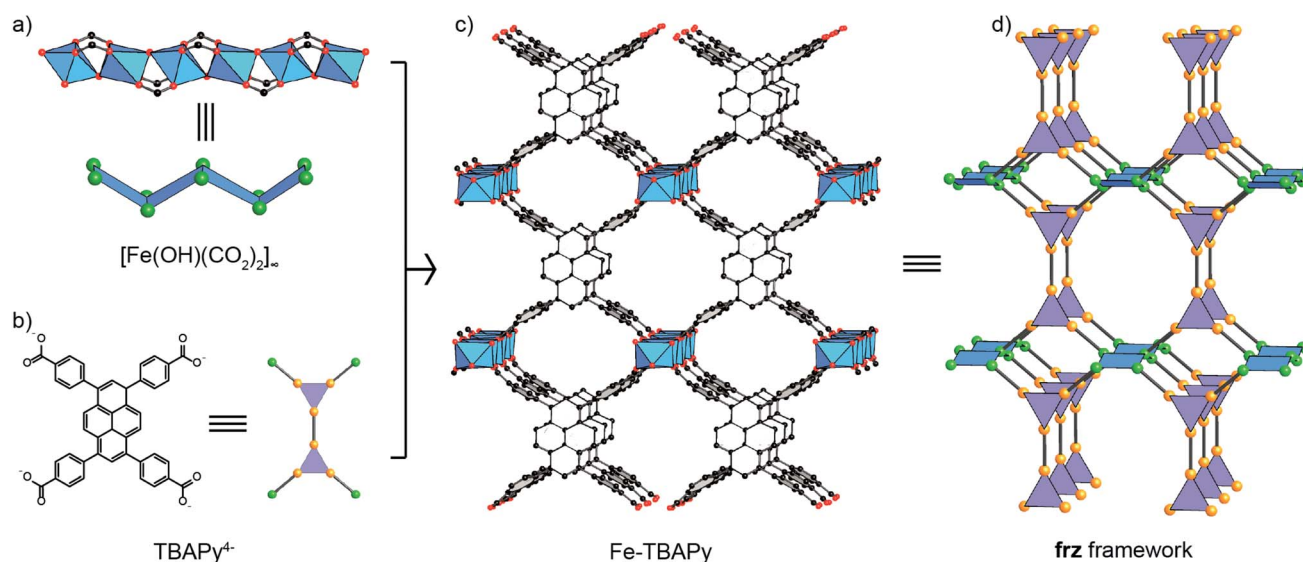

Fig. 1 Fe-TBAPy is constructed from $[Fe(OH)(CO_2)_2]_\infty$ rod-shaped SBUs (a), linked by tetratopic $TBAPy^{4-}$ linkers (b) to expand into the **frz** topologically based framework (c and d). Atom colors: Fe, blue polyhedra; C, black; O, red. All hydrogen atoms are omitted for clarity.

framework (Fig. 1c and d) highlighted by 7 Å channel and 3.4 Å pores sandwiching between the pyrene cores of TBAPy[4−] (Fig. S4†).[45,46]

Fourier transform-infrared (FT-IR) spectroscopy analysis of the activated sample showed the structural stability with the $\nu_{C=O}$ stretching peak of coordinated carboxylate at 1605 cm^{−1} (Fig. S5†). Elemental microanalysis (EA) confirmed the proposed chemical formula of Fe-TBAPy to be $Fe_2(OH)_2(TBAPy)\cdot$ $4.4H_2O$: C, 58.46; H, 3.41; N, 0%. Found: C, 58.5; H, 3.69; N, 0.31%. The thermal stability and the permanent porosity of Fe-TBAPy were further investigated by thermogravimetric analysis (TGA) and 77 K N_2 adsorption measurements. TGA showed that Fe-TBAPy is stable up to 300 °C with a small weight percentage loss (<4.5 wt%) (Fig. S6†). Furthermore, the weight percentage of the residual oxide (assigned to Fe_2O_3) is 22.2 wt%, which is consistent with the theoretical value calculated from the modelled structure (19.5 wt%) (Fig. S6†). N_2 isotherm of Fe-TBAPy exhibits reversible uptake, with BET (Langmuir) surface area of 650 m[2] g^{−1} (703 m[2] g^{−1}) (Fig. S7†). These values are in agreement with the theoretically predicted surface area (Materials Studio 8.0; Langmuir SA = 820 m[2] g^{−1}). Furthermore, pore size distribution analysis derived from N_2 isotherm confirmed the existence of the 7 Å channel in Fe-TBAPy (Fig. S8†).

Subsequently, the activated Fe-TBAPy were immersed in the water solution of HCl or KOH with pH from 2 to 10 for 5 days. Following this, these samples were exchanged with DMF, MeOH, CH_2Cl_2, and activated under dynamic vacuum at room temperature. As shown in Fig. S9,† the PXRD profile of the water-immersed samples showed the peak-shifts compared with the PXRD pattern of the activated sample. Further Pawley refinement against the experimental profile of these samples indicated the maintenance of the periodic structure; however, the slight changes of the unit cell parameters were found (Fig. S9†). Indeed, such structural flexibilities are also observed for [In$_2$(OH)$_2$(TBAPy)] and common Fe-based MOFs.[42,43,47] FT-IR analysis of water-immersed samples also confirmed the

maintenance of the coordinated bond with the characterized peak at 1605 cm^{−1} (Fig. S10†). Furthermore, the absence of peaks of free carboxylic acid implied the full maintenance of the atomic connectivity without exfoliation (Fig. S10†). This data showed that Fe-TBAPy is stable in acidic and basic water and such property endow this material to be employed as the oxidative catalyst under harsh conditions, in which common MOFs cannot retain the structure.[48]

Catalytic activity

Since the catalysis activity of MOFs strongly depends on the constituent metal SBUs[41,49] and/or the adsorption and diffusion of the substrates onto the internal surface,[50,51] the materials, whose structures are characterized by substrate-fitting pores, tend to show the enhancing or selective catalysis.[51–53] Inspired by In$_2$(OH)$_2$(TBAPy) compound, whose structure is found to allow the toluene molecules to sandwich into the narrow pores between the pyrene cores of TBAPy[4−],[42] we anticipated that 3.4 Å pores sandwiching inside Fe-TBAPy could be the strong adsorption-sites for benzene because of the strong π–π interaction of this substrate and pyrene cores of TBAPy[4−]. This consequently boost the catalysis activity of Fe-TBAPy catalyst for the benzene hydroxylation reaction (Fig. S4†).

To take this further, the benzene hydroxylation reactions using Fe-TBAPy catalyst were evaluated according to a published procedure; however, with the slight modification of reaction parameters.[34] Initially, the reaction was carried out at room temperature, in which the catalyst (4.3 mol%), benzene (50 μL) and H_2O_2 (30 wt%, 100 μL) were used. The reaction resulted in 36% GC yield for phenol after 24 h while the byproducts were not detected (Table S2, entry 1†). Increasing the reaction temperature to 50 °C resulted in an increase of phenol yield to 40.1% with 94.5% selectivity found (Table S2, entry 2†). In comparison, MIL-100(Fe) showed 30.6% benzene conversion after performing the catalysis reaction for 24 h (used equal mol% of iron metal with Fe-TBAPy),[34] the high phenol yield catalyzed by Fe-TBAPy, therefore, indicated the outperformed catalysis activity of Fe-TBAPy over MIL-100(Fe). We further carried out the catalysis reactions using 1 mol% Fe-TBAPy with increasing temperature and amount of H_2O_2 (100, 300 and 600 μL) to maximize the performance of Fe-TBAPy. This resulted in the phenol yield of 17.9%, 33.9%, and 57.8%, respectively, at 70 °C and 24 h (Fig. 3 and Table S2, entry 6, 7 and 8†). Extending the reaction time resulted in the steady increase of phenol yield until 33 h with 45.6 and 64.5% yield detected (corresponding to 300 and 600 μL H_2O_2, respectively) (Fig. 3 and Table S2, entry 9 & 16†). Interestingly, gas chromatography (GC) analysis showed the high phenol selectivity of 92.9% at the optimized condition (Fig. S11 and Table S2, entry 9†). In addition, we found that the catalysis activity of Fe-TBAPy is comparable with that of the best-performing catalysts for benzene hydroxylation such as FeOCl (43.5%),[1] V–Si–ZSM-22 (30.8%),[3] TS-1 (29.5%),[54] PMO-1 (27.4%),[55] Cu$_2$O-8/dG (19.4%),[9] CuCr$_2$O$_4^{RB}$ (65%)[5] (Table S3†).

The control experiment was further carried out to verify the heterogeneous nature of Fe-TBAPy. As expected, phenol
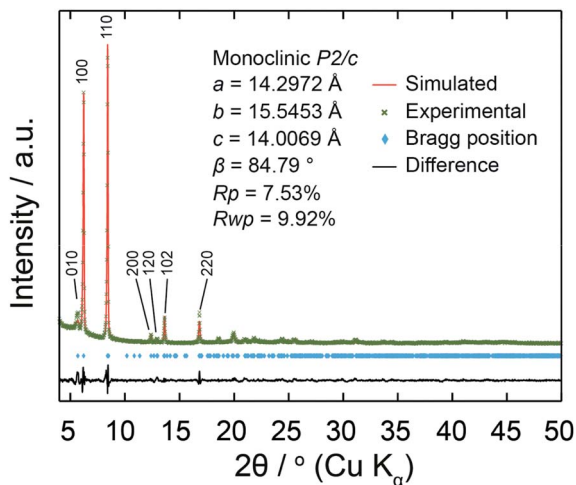

Fig. 2 Experimental (green) and refined (red) PXRD patterns of activated Fe-TBAPy after Rietveld refinement. The difference plot (black) and Bragg positions (blue) are also shown. Full range Rietveld refinement data ($2\theta = 2–80°$) is provided in the ESI (Section S4†).

Monoclinic P2/c
a = 14.2972 Å
b = 15.5453 Å
c = 14.0069 Å
β = 84.79 °
Rp = 7.53%
Rwp = 9.92%

Legend: Simulated, Experimental (×), Bragg position (♦), Difference

Axis labels: Intensity / a.u. (y-axis); 2θ / ° (Cu K$_\alpha$) (x-axis)
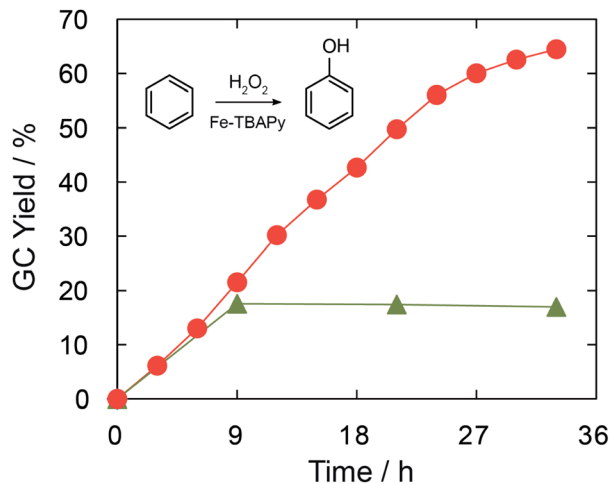
Fig. 3 GC yield of phenol in the presence of Fe-TBAPy catalyst (red cycle) and the control reaction with the removal of the catalyst after 9 h (green triangle).

Table 1 The hydroxylation of benzene performed in our laboratory utilizing different iron-based catalysts[b]

Entry	Catalysts[c]	Y_{phenol}[a]/%	S/%
1	Fe-TBAPy	64.5 ± 0.64	92.9
2	MIL-100(Fe)	45.3 ± 1.67	93.8
3	MIL-126	42.1 ± 0.97	93
4	VNU-20	48.1 ± 1.22	93.8
5	MIL-68(Fe)	35.4 ± 0.53	91.6
6	MIL-88(Fe)	38.2 ± 1.27	92.4
7	$FeCl_3 \cdot 6H_2O$	5.9 ± 0.43	100
8	$FeCl_2$	6.7 ± 0.31	100
9	$FeSO_4 \cdot 7H_2O$	5.1 ± 0.11	100

[a] Y_{phenol}: GC yield of phenol; S: phenol selectivity. [b] Reaction conditions: benzene (50 µL), H_2O_2 (30 wt%, 600 µL), 70 °C and 33 h. [c] Equal mol% Fe metal in each catalysts were used for comparison.

formation was no longer detected after the isolation of Fe-TBAPy from the reaction medium. This implied the benzene hydroxylation reaction catalysed by Fe-TBAPy and the contribution of the iron metal leached out from Fe-TBAPy is negligible (Fig. 3). The durability of Fe-TBAPy as a catalyst was further evaluated by carrying out the catalysis experiments for up to five cycles. Experimental results indicated that Fe-TBAPy could be reused without a significant reduction in catalytic activity. Specifically, up to 60.9% GC yield of phenol was found after the fifth cycle using the recycled Fe-TBAPy sample (Fig. 4). Moreover, the structural maintenance without significant degradation of Fe-TBAPy after consecutive catalytic experiments was confirmed by FT-IR and PXRD measurements (Fig. S13 and S14†).

The advantage of using Fe-TBAPy for benzene hydroxylation was further demonstrated by comparing the catalysis activity with the other Fe-based MOFs such as MIL-100(Fe) and MIL-126, which are characterized by both the large pore and high surface area.[37,38] As shown in Table 1 (entry 2 & 3), the catalysis
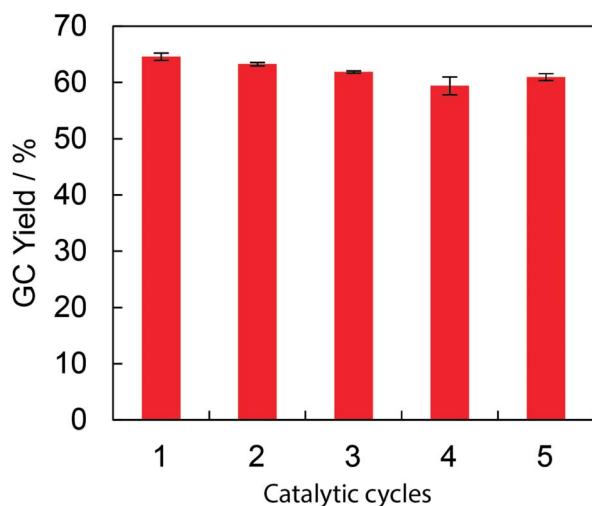
activity of Fe-TBAPy is significantly higher than those materials. We further synthesized and tested the catalysis activity of Fe-based MOFs constructed from the rod-shaped SBUs (e.g. MIL-68(Fe) and VNU-20). Accordingly, VNU-20 showed slightly lower catalysis activity comparing to Fe-TBAPy (Table 1, entry 4), whereas MIL-68(Fe) exhibited poor catalysis activity (Table 1, entry 5). Additionally, the catalysis reaction using MIL-88(Fe) and the homogeneous iron salts also showed poor performance (entry 6–9). Since Fe-based MOFs (MIL-100(Fe), MIL-126, and MIL-68(Fe)), whose structure are either characterized by large pore size and high surface area or built from the similar $[Fe(OH)(CO_2)_2]_\infty$ SBUs with Fe-TBAPy,[39] showed poor catalysis activity, the high performance of Fe-TBAPy implied the presence of the narrow pores in Fe-TBAPy actually enhancing the catalysis activity of this material for benzene hydroxylation.

4. Conclusions

In summary, a new Fe-based MOF, termed Fe-TBAPy, is succeeded to synthesize and characterize. Structural analysis revealed that Fe-TBAPy is constructed from $[Fe(OH)(CO_2)_2]_\infty$ rod-shaped SBUs, which are linked by TBAPy[4−] to extend into the three-dimensional **frz** topological framework. The structure of Fe-TBAPy is highlighted by 7 Å channel and 3.4 Å pores sandwiching between the pyrene cores of TBAPy[4−]. With this structural feature, Fe-TBAPy was employed as the catalyst for hydroxylation of benzene. The catalytic tests resulted in the optimized phenol yield and selectivity of 64.5% with 92.9%, respectively. Remarkably, this value is found to be higher than that of iron-based MOFs (e.g. MIL-100(Fe), MIL-126, MIL-68(Fe), MIL-88(Fe) and VNU-20) and comparable with that of the best-performing catalysts for benzene hydroxylation. We believe that this experience will inspire the design and synthesis of new porous frameworks, for examples, via the reticular expansion or mixed metals approach to maximize the catalysis performance for benzene hydroxylation.[56,57]

Conflicts of interest

There are no conflicts to declare.

Fig. 4 Catalyst recycling studies of Fe-TBAPy.

Acknowledgements

References

1 A. E. ElMetwally, G. Eshaq, F. Z. Yehia, A. M. Al-Sabagh and S. Kegnæs, *ACS Catal.*, 2018, **8**, 10668–10675.

2 S. S. Acharyya, S. Ghosh, R. Tiwari, C. Pendem, T. Sasaki and R. Bal, *ACS Catal.*, 2015, **5**, 2850–2858.

3 Y. Zhou, Z. Ma, J. Tang, N. Yan, Y. Du, S. Xi, K. Wang, W. Zhang, H. Wen and J. Wang, *Nat. Commun.*, 2018, **9**, 2931–2941.

4 H. Wang, C. Wang, M. Zhao, Y. Yang, L. Fang and Y. Wang, *Chem. Eng. Sci.*, 2018, **177**, 399–409.

5 S. S. Acharyya, S. Ghosh and R. Bal, *ACS Appl. Mater. Interfaces*, 2014, **6**, 14451–14459.

6 T. Jiang, W. Wang and B. Han, *New J. Chem.*, 2013, **37**, 1654–1664.

7 P. Borah, A. Datta, K. T. Nguyen and Y. Zhao, *Green Chem.*, 2016, **18**, 397–401.

8 M. Shahami, K. M. Dooley and D. F. Shantz, *J. Catal.*, 2018, **368**, 354–364.

9 J. He, M. Zhang, A. Primo, H. García and Z. Li, *J. Mater. Chem. A*, 2018, **6**, 19782–19787.

10 T. Zhang, D. Zhang, X. Han, T. Dong, X. Guo, C. Song, R. Si, W. Liu, Y. Liu and Z. Zhao, *J. Am. Chem. Soc.*, 2018, **140**, 16936–16940.

11 V. I. Pârvulescu, D. Dumitriu and G. Poncelet, *J. Mol. Catal. A: Chem.*, 1999, **140**, 91–105.

12 H. Furukawa, K. E. Cordova, M. O'Keeffe and O. M. Yaghi, *Science*, 2013, **341**, 1230444, DOI: 10.1126/science.1230444.

13 K. Adil, Y. Belmabkhout, R. S. Pillai, A. Cadiau, P. M. Bhatt, A. H. Assen, G. Maurin and M. Eddaoudi, *Chem. Soc. Rev.*, 2017, **46**, 3402–3430.

14 H. Furukawa, F. Gándara, Y.-B. Zhang, J. Jiang, W. L. Queen, M. R. Hudson and O. M. Yaghi, *J. Am. Chem. Soc.*, 2014, **136**, 4369–4381.

15 C. A. Rowland, G. R. Lorzing, E. J. Gosselin, B. A. Trump, G. P. A. Yap, C. M. Brown and E. D. Bloch, *J. Am. Chem. Soc.*, 2018, **140**, 11153–11157.

16 X. Meng, H.-N. Wang, S.-Y. Song and H.-J. Zhang, *Chem. Soc. Rev.*, 2017, **46**, 464–480.

17 M. V. Nguyen, T. H. N. Lo, L. C. Luu, H. T. T. Nguyen and T. N. Tu, *J. Mater. Chem. A*, 2018, **6**, 1816–1821.

18 T. H. N. Lo, M. V. Nguyen and T. N. Tu, *Inorg. Chem. Front.*, 2017, **4**, 1509–1516.

19 K. G. M. Laurier, F. Vermoortele, R. Ameloot, D. E. De Vos, J. Hofkens and M. B. J. Roeffaers, *J. Am. Chem. Soc.*, 2013, **135**, 14488–14491.

20 T. N. Tu, M. V. Nguyen, H. L. Nguyen, B. Yuliarto, K. E. Cordova and S. Demir, *Coord. Chem. Rev.*, 2018, **364**, 33–50.

21 L. E. Kreno, K. Leong, O. K. Farha, M. Allendorf, R. P. V. Duyne and J. T. Hupp, *Chem. Rev.*, 2012, **112**, 1105–1125.

22 Z. Sun, S. Yu, L. Zhao, J. Wang, Z. Li and G. Li, *Chem. - Eur. J.*, 2018, **24**, 10829–10839.

23 L. Yang, C. Lian, X. Li, Y. Han, L. Yang, T. Cai and C. Shao, *ACS Appl. Mater. Interfaces*, 2017, **9**, 17208–17217.

24 S. Wuttke, M. Lismont, A. Escudero, B. Rungtaweevoranit and W. J. Parak, *Biomaterials*, 2017, **123**, 172–183.

25 R. Freund, U. Lächelt, T. Gruber, B. Rühle and S. Wuttke, *ACS Nano*, 2018, **12**, 2094–2105.

26 Z. R. Herm, B. M. Wiers, J. A. Mason, J. M. van Baten, M. R. Hudson, P. Zajdel, C. M. Brown, N. Masciocchi, R. Krishna and J. R. Long, *Science*, 2013, **340**, 960–964.

27 J. A. Mason, J. Oktawiec, M. K. Taylor, M. R. Hudson, J. Rodriguez, J. E. Bachman, M. I. Gonzalez, A. Cervellino, A. Guagliardi, C. M. Brown, P. L. Llewellyn, N. Masciocchi and J. R. Long, *Nature*, 2015, **527**, 357–361.

28 T. N. Tu, N. Q. Phan, T. T. Vu, H. L. Nguyen, K. E. Cordova and H. Furukawa, *J. Mater. Chem. A*, 2016, **4**, 3638–3641.

29 T. A. To, Y. H. Vo, H. T. T. Nguyen, P. T. M. Ha, S. H. Doan, T. L. H. Doan, S. Li, H. V. Le, T. N. Tu and N. T. S. Phan, *J. Catal.*, 2019, **370**, 11–20.

30 D. J. Xiao, E. D. Bloch, J. A. Mason, W. L. Queen, M. R. Hudson, N. Planas, J. Borycz, A. L. Dzubak, P. Verma, K. Lee, F. Bonino, V. Crocella, J. Yano, S. Bordiga, D. G. Truhlar, L. Gagliardi, C. M. Brown and J. R. Long, *Nat. Chem.*, 2014, **6**, 590–595.

31 D. J. Xiao, J. Oktawiec, P. J. Milner and J. R. Long, *J. Am. Chem. Soc.*, 2016, **138**, 14371–14379.

32 S. H. Doan, V. H. H. Nguyen, T. H. Nguyen, P. H. Pham, N. N. Nguyen, A. N. Q. Phan, T. N. Tu and N. T. S. Phan, *RSC Adv.*, 2018, **8**, 10736–10745.

33 S. H. Doan, N. K. Q. Tran, P. H. Pham, V. H. H. Nguyen, N. N. Nguyen, P. T. M. Ha, S. Li, H. V. Le, N. T. H. Le, T. N. Tu and N. T. S. Phan, *Eur. J. Org. Chem.*, 2019, **2019**, 2382–2389.

34 D. Wang, M. Wang and Z. Li, *ACS Catal.*, 2015, **5**, 6852–6857.

35 B. Xu, Z. Chen, B. Han and C. Li, *Catal. Commun.*, 2017, **98**, 112–115.

36 M. O'Keeffe, M. A. Peskov, S. J. Ramsden and O. M. Yaghi, *Acc. Chem. Res.*, 2008, **41**, 1782–1789.

37 P. Horcajada, S. Surblé, C. Serre, D.-Y. Hong, Y.-K. Seo, J.-S. Chang, J.-M. Grenèche, I. Margiolaki and G. Férey, *Chem. Commun.*, 2007, 2820–2822.

38 M. Dan-Hardi, H. Chevreau, T. Devic, P. Horcajada, G. Maurin, G. Férey, D. Popov, C. Riekel, S. Wuttke, J.-C. Lavalley, A. Vimont, T. Boudewijns, D. de Vos and C. Serre, *Chem. Mater.*, 2012, **24**, 2486–2492.

39 A. Fateeva, P. Horcajada, T. Devic, C. Serre, J. Marrot, J. M. Grenèche, M. Morcrette, J. M. Tarascon, G. Maurin and G. Férey, *Eur. J. Inorg. Chem.*, 2010, **68**, 3789–3794.

40 S. Surblé, C. Serre, C. Mellot-Draznieks, F. Millange and G. Férey, *Chem. Commun.*, 2006, 284–286.

41 P. H. Pham, S. H. Doan, H. T. T. Tran, N. N. Nguyen, A. N. Q. Phan, H. V. Le, T. N. Tu and N. T. S. Phan, *Catal. Sci. Technol.*, 2018, **8**, 1267–1271.

42 K. C. Stylianou, R. Heck, S. Y. Chong, J. Bacsa, J. T. A. Jones, Y. Z. Khimyak, D. Bradshaw and M. J. Rosseinsky, *J. Am. Chem. Soc.*, 2010, **132**, 4119–4130.

43 P. L. Llewellyn, P. Horcajada, G. Maurin, T. Devic, N. Rosenbach, S. Bourrelly, C. Serre, D. Vincent, S. Loera-Serna, Y. Filinchuk and G. Férey, *J. Am. Chem. Soc.*, 2009, **131**, 13002–13008.

44 S. Bourrelly, P. L. Llewellyn, C. Serre, F. Millange, T. Loiseau and G. Férey, *J. Am. Chem. Soc.*, 2005, **127**, 13519–13521.

45 R. J. Li, M. Li, X. P. Zhou, D. Li and M. O'Keeffe, *Chem. Commun.*, 2014, **50**, 4047–4049.

46 A. Schoedel, M. Li, D. Li, M. O'Keeffe and O. M. Yaghi, *Chem. Rev.*, 2016, **116**, 12466–12535.

47 S. Surble, C. Serre, C. Mellot-Draznieks, F. Millange and G. Ferey, *Chem. Commun.*, 2006, 284–286.

48 A. J. Howarth, Y. Liu, P. Li, Z. Li, T. C. Wang, J. T. Hupp and O. K. Farha, *Nat. Rev. Mater.*, 2016, **1**, 15018–15033.

49 Y.-B. Huang, J. Liang, X.-S. Wang and R. Cao, *Chem. Soc. Rev.*, 2017, **46**, 126–157.

50 H. T. T. Nguyen, T. N. Tu, M. V. Nguyen, T. H. N. Lo, H. Furukawa, N. N. Nguyen and M. D. Nguyen, *ACS Appl. Mater. Interfaces*, 2018, **10**, 35462–35468.

51 J. M. Roberts, B. M. Fini, A. A. Sarjeant, O. K. Farha, J. T. Hupp and K. a Scheidt, *J. Am. Chem. Soc.*, 2012, **134**, 3334–3337.

52 H. Fei, D. L. Rogow and S. R. J. Oliver, *J. Am. Chem. Soc.*, 2010, **132**, 7202–7209.

53 W. Zhang, G. Lu, C. Cui, Y. Liu, S. Li, W. Yan, C. Xing, Y. R. Chi, Y. Yang and F. Huo, *Adv. Mater.*, 2014, **26**, 4056–4060.

54 P. T. Tanev, M. Chibwe and T. J. Pinnavaia, *Nature*, 1994, **368**, 321–323.

55 P. Borah, X. Ma, K. T. Nguyen and Y. Zhao, *Angew. Chem., Int. Ed.*, 2012, **51**, 7756–7761.

56 H. Furukawa, U. Müller and O. M. Yaghi, *Angew. Chem., Int. Ed.*, 2015, **54**, 3417–3430.

57 L. J. Wang, H. Deng, H. Furukawa, F. Gándara, K. E. Cordova, D. Peri and O. M. Yaghi, *Inorg. Chem.*, 2014, **53**, 5881–5883.